2018 European Control Conference (ECC)
June 12-15, 2018. Limassol, Cyprus

Active and reactive power regulation in single-phase PV inverters

Domingo Biel and Jacquelien M.A. Scherpen

Abstract— **This work presents the design of a control to regulate the active and the reactive power in single-phase PV inverters. The control is composed by an inner loop with a passivity-based control in charge to track the current reference generated by the outer loop and PI controllers in the outer loop that regulate the power injection of the PV inverter. The passivity-based control ensures global asymptotic convergence of the tracking error to zero and the PV inverter shows robust current tracking with fast dynamics. Furthermore, a model of the overall control system is derived and the PI controllers parameters design guidelines which guarantee local asymptotic stability and robustness with respect to the unknown grid impedance are also provided. Numerical simulations when the power references, the PV irradiance or the grid impedance are changed validate the control performance.**

I. Introduction

The increase of the number of PV installations has great impact on the electricity network, makes the grid more decentralized and the grid quality can be seriously affected. For this reason, nowadays some new functionalities are required for the PV systems in order to keep the grid (at least at the connection point of the PV system) in compliance with the quality standards. One of these new requirements is the control of the active and the reactive power that the inverter injects to the grid.

The regulation of the reactive power and the active power is usually achieved by the design of a current loop that ensures the injection of the proper grid current that provides the desired active and reactive power. The controller can be designed by using linear control techniques in a rotating frame dq [1], [2], [3] or in a time-variant framework [4], [5], [6], [7], [8], [9] or appying nonlinear control techniques as Lyapunov-based control [10] or passivity-based control [11].

The power references of the current control are given by an external controller which is communicated with the local PV inverter controller. The strategy allows the application of optimization procedures in order to set the power references for a given network. The optimization control is usually applied with the goal to support the voltage of the power networks assuming that the number nodes and the impedances among them are known. The calculated power references are then sent to the local controllers that have to properly track these settings. Finally, the power regulation is achieved by controlling the amplitude of the delivered current to the grid and by properly phase shifting the current with respect to the voltage at the connection point, which it is also phase shifted with respect to the ideal sinusoidal grid due to the impedance between both of them. This impedance depends on the usage of the grid, and is thus unknown.

In order to ensure a robust power regulation with respect to the grid impedance, this work includes an outer loop in charge to deliver the references to the current loop. The outer loop design assumes that the internal PV inverter variables reach their steady-state regime; but although this assumption, the dynamical description of the complete system is nonlinear and the controllers design is even worsened by the unknown impedance that exists between the connection point and the grid source. In order to overcome the aforementioned problems, in this work we study and develop the nonlinear model, approximate it when steady-state assumptions are valid, and then use a linearisation procedure for the designs of the PI controllers to guarantee local closed loop asymptotic stability. Moreover, PI parameters are designed to obtain smooth and brief transients when the grid impedance varies, thus ensuring the proper power regulation over the whole working range without any measure or estimation of the grid impedance.

The remainder of the paper is organized as follows. In Section II, we state the problem solved in this communication. Section III is devoted to introduce the passivity-control which tracks the current reference in order to inject the desired active and reactive power to the grid and to analyse the stability of the PV output voltage dynamics. The control scheme for the active and the reactive power regulation is studied in Section IV. A model of the system is derived and the design of the PI controllers parameters to guarantee local asymptotic stability are provided. The control is evaluated by means of numerical simulations in three different scenarios; namely, when the power references change, when the PV irradiance varies and when the grid impedance suffer some variations. The results presented in section V confirm the expected properties of stability, fast current tracking and robustness of the control. Finally, conclusions are drawn in the last section of this article.

II. Problem statement

The Fig. 1 presents a PV inverter connected to a non-ideal grid (modelled by an impedance and an ideal sinusoidal source). The state equations (in averaged values) of the PV inverter are:

$$C\dot{z}_1 = -uz_2 + f_{pv}(z_1) \tag{1a}$$

$$L\dot{z}_2 = uz_1 - v_{CP} \tag{1b}$$

D. Biel is with the Institute of Industrial and Control Engineering and the Department of Electronic Engineering, Universitat Politecnica de Catalunya, Spain domingo.biel@upc.edu

J.M.A. Scherpen is with the Jan C. Willems Center for Systems and Control, Engineering and Technology Institute (ENTEG), Faculty of Science an Engineering, University of Groningen, The Netherlands j.m.a.scherpen@rug.nl

where z_1 and z_2 correspond to the capacitor voltage and the inductor current, respectively, L is the inductance, C is the capacitance, $u \in [-1, 1]$ is the control (duty cycle), $v_{CP} = A_{CP}\sin(\omega t)$ is the voltage at the connection point and $f_{pv}(z_1) = \Lambda - \Psi e^{(\alpha z_1)}$ is the current delivered by the PV array. Here Λ represents the part of the PV generator current that depends on the solar radiation, and α and Ψ are positive parameters of the PV generator. The parameters L and C are assumed to be known constants. The PV inverter has to be controlled to perform two main tasks:

1) To deliver the desired active power to the grid (for instance, the active power reference value could be given by a Maximum Power Point Tracker (MPPT)).
2) To control the injected reactive power to the grid.

The aforementioned goals are achieved by the design of the control system shown in the Fig. 1. The control structure is composed by two different loops, namely:

1) An inner loop to control the injected grid current in order to track the signal delivered by the reference generator block that, in turn, provides the required active and reactive power. A passivity-based controller, which ensures global stability of the loop, is designed for this purpose.
2) An outer loop in charge of controlling the active and the reactive power delivered to the grid. PI controllers are designed to perform this task.

The following sections are devoted to model the control system and to analyse the stability conditions of each loop.

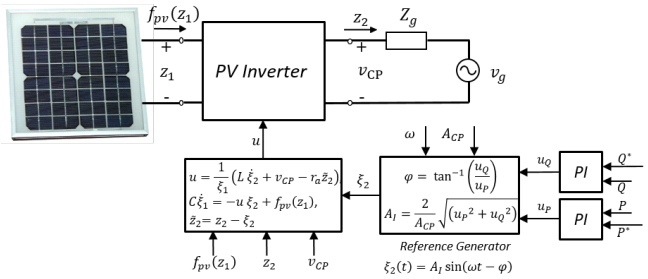

Fig. 1. Control scheme of the passivity-based control of the active and the reactive power in PV inverters connected to the grid with outer PI controllers.

III. Current control

A. Passivity-based control

Passivity-based control has been successfully applied to power converters ([12], [13], [14], [15], [16], [17], [18], among others). This work uses the passivity-based control proposed in [11] and includes a detailed proof of stability. The block diagram depicted in the Fig. 1 shows the passivity-based controller scheme. The controller uses a reference generator which generates the current reference, $\xi_2(t) = A_I \sin(\omega t - \theta)$, to be tracked by the PV inverter. The values of the amplitude and phase of the current reference are calculated applying the well-known expressions that relate both values with the active and the reactive power:

$$A_I = 2\frac{\sqrt{P^2 + Q^2}}{A_{CP}},\ \theta = \arctan\left(\frac{Q}{P}\right). \tag{2}$$

The controller determines the control signal from the values of the current reference, $\xi_2(t)$, the current injected to the grid, z_2, the PV array current, $f_{pv}(z_1)$, and the voltage at the connection point, v_{CP}.

Proposition 1: Consider the system defined by (1), where L and C are known constant parameters. A nonlinear dynamic feedback passivity-based controller is given by

$$u = \frac{(L\dot{\xi}_2 + v_{CP} - r_a(z_2 - \xi_2))}{\xi_1}, \tag{3a}$$

$$C\dot{\xi}_1 = -u\xi_2 + f_{pv}(z_1), \tag{3b}$$

being the reference current $\xi_2(t) = A_I \sin(\omega t - \theta)$ and the controller parameter $r_a > 0$. Under these conditions and assuming $\xi_1(t) > 0$, the controller solves the tracking problem of the grid injected current, i.e., $\lim_{t\to\infty} z_2(t) = \xi_2(t)$.

Proof: Defining the error variables $\tilde{z}_1 = z_1 - \xi_1$, $\tilde{z}_2 = z_2 - \xi_2$, the system (1) can be rewritten as:

$$C\dot{\tilde{z}}_1 = -u\tilde{z}_2 - u\xi_2 + f_{pv}(z_1) - C\dot{\xi}_1, \tag{4a}$$

$$L\dot{\tilde{z}}_2 = u\tilde{z}_1 + u\xi_1 - v_{CP} - L\dot{\xi}_2, \tag{4b}$$

which, replacing the controller equations, results in

$$C\dot{\tilde{z}}_1 = -u\tilde{z}_2, \tag{5a}$$

$$L\dot{\tilde{z}}_2 = u\tilde{z}_1 - r_a\tilde{z}_2, \tag{5b}$$

In order to prove the stability of the error system, consider the following lower bounded Lyapunov function:

$$V = \frac{1}{2}C\tilde{z}_1^2 + \frac{1}{2}L\tilde{z}_2^2, \tag{6}$$

where the time derivative along the trajectories of (5) is given by

$$\dot{V} = \tilde{z}_1(-u\tilde{z}_2) + \tilde{z}_2(u\tilde{z}_1 - r_a\tilde{z}_2) = -r_a\tilde{z}_2^2 \leq 0, \tag{7}$$

which indicates that $\dot{V}$ is a negative semi-definite function and hence the variables $\tilde{z}_1$ and $\tilde{z}_2$ are also bounded. Furthermore, following Barbalat's lemma, the global asymptotic convergence of the tracking error $\tilde{z}_2$ to zero is guaranteed because the boundedness of u, $\tilde{z}_1$ and $\tilde{z}_2$ implies the boundedness of $\dot{\tilde{z}}_2$ and therefore the uniform continuity of $\dot{V}$. Notice that the boundedness of the control signal u is ensured since all the involved variables are bounded and the controller variable ξ_1 is assumed bounded away from zero. Moreover, when the perfect tracking is achieved, $\tilde{z}_2 = 0$, the error system simplifies in $\dot{\tilde{z}}_1 = 0$ and $u\tilde{z}_1 = 0$ and, taking into account that the control signal u is a time variant signal, the last expression implies that $\tilde{z}_1 = 0$ and $\xi_1 = z_1$. ■

Remark 1: Numerical simulations show that ξ_1 converges quickly to z_1 when the value of $\xi_1(0)$ is selected to be equal to the initial condition of the PV output voltage.

B. Internal dynamics of the PV inverter capacitor voltage

The differential equation that defines the dynamics of the PV inverter capacitor voltage is given by the balance power equation:

$$Cz_1\dot{z}_1 = z_1 f_{pv}(z_1) - (L\dot{z}_2 + v_{CP})z_2, \tag{8}$$

which, assuming that the reference current is perfectly tracked, $z_2(t) = \xi_2(t)$, and recalling that the voltage at the connection point is $v_{CP} = A_{CP}\sin(\omega t)$, can be rewritten as:

$$Cz_1\dot{z}_1 = F(z_1) - P + \varphi(t), \tag{9}$$

where $\varphi(t) = \frac{A_{CP}A_I}{2}\cos(2\omega t - \theta) - \frac{LA_I^2\omega}{2}\sin(2\omega t - 2\theta)$, and $F(z_1) = z_1 f_{pv}(z_1) > 0$ represents the PV power.

The equation (9) has no explicit solutions. Assuming that there exist some $\frac{\pi}{\omega}$-periodic solutions, z_1^*, then $\frac{\omega}{\pi}\int_0^{\frac{\pi}{\omega}} \dot{z}_1^* dt = 0$ and $\frac{\omega}{\pi}\int_0^{\frac{\pi}{\omega}} \varphi(t)dt = 0$, and the averaged values will fulfil the equation $\overline{F(z_1^*)} = P$, where $\overline{F(z_1^*)} = \frac{\omega}{\pi}\int_0^{\frac{\pi}{\omega}} F(z_1^*)dt$. Therefore, when $\max\big(F(z_1)\big) > P$ and the amplitude of the harmonics of z_1^* are low enough, (9) will have two different solutions. These solutions are located at both sides of the value at the maximum power point of the PV array.

Proposition 2: Assuming that the PV inverter operates in a perfect tracking mode, $z_2(t) = A_I\sin(\omega t - \theta)$, the active power injected to the grid is lower than the maximum power of the PV array and the PV inverter capacitance is designed such that the ripple of z_1 can be neglected with respect its average value, then the PV output voltage stabilizes to the solution of (9) located to the right of the PV maximum power point.

Proof: In order to analyse the power equation, the variable $\epsilon = 0.5Cz_1^2$ is defined. Therefore, the notation of (9) is simplified as:

$$\dot{\epsilon} = F(\epsilon) - P + \varphi(t) \tag{10}$$

where $F(\epsilon) = \sqrt{\frac{2\epsilon}{C}}(\Lambda - \Psi e^{(\alpha\sqrt{\frac{2\epsilon}{C}})}) > 0$. This function has a maximum which can be obtained by solving the equation:

$$\dot{F}(\epsilon) = \frac{1}{\sqrt{2C\epsilon}}\big(\Lambda - \Psi e^{(\alpha\sqrt{\frac{2\epsilon}{C}})}\big(1 + \big(\alpha\sqrt{\frac{2\epsilon}{C}}\big)\big)\big) = 0 \tag{11}$$

which has only one solution, ϵ_{MPP}, corresponding to the PV array maximum power point. The equation (11) can be rewritten as:

$$\Lambda - \Psi e^{(y_{MPP}-1)} y_{MPP} = 0, \tag{12}$$

where the variable $y = 1 + \alpha\sqrt{\frac{2\epsilon}{C}}$ has been defined. The solution of (12) responds to a Lambert-W function and it can be expressed as $y_{MPP} = W(\frac{\Lambda}{\Psi}e)$.

From (9) and the discussion below (9) it follows that there exist some $\frac{\pi}{\omega}$-periodic solutions, ϵ^*, then $\frac{\omega}{\pi}\int_0^{\frac{\pi}{\omega}} \dot{\epsilon}^* dt = 0$ and $\frac{\omega}{\pi}\int_0^{\frac{\pi}{\omega}} \varphi(t)dt = 0$, and the averaged values will fulfil the equation $\overline{F(\epsilon^*)} = P$, where $\overline{F(\epsilon^*)} = \frac{\omega}{\pi}\int_0^{\frac{\pi}{\omega}} F(\epsilon^*)dt$. Therefore, when $\max\big(F(\epsilon)\big) > P$ and the amplitude of the harmonics of ϵ^* are low enough, (10) will have two different solutions. Recalling the expression of (11) one can easily find out that $\dot{F}(\epsilon) > 0$ for $0 < \epsilon < \epsilon_{MPP}$ and $\dot{F}(\epsilon) < 0$ for $\epsilon_{MPP} < \epsilon < \epsilon_{max}$, being ϵ_{max} the value of ϵ which fulfils $F(\epsilon) = 0$. Hence, the solutions of (10) are located, one on the left side of ϵ_{MPP}, $\epsilon^* = \epsilon_L^*$, and the other on the right side of ϵ_{MPP}, $\epsilon^* = \epsilon_R^*$.

The following Lyapunov function candidate is defined: $V = 0.5\tilde{\epsilon}^2$, where $\tilde{\epsilon} = \epsilon - \epsilon^*$. The time derivative of the Lyapunov function is $\dot{V} = \tilde{\epsilon}\dot{\tilde{\epsilon}} = \tilde{\epsilon}(F(\epsilon) - F(\epsilon^*))$. Therefore, taking into account the previous results, the following stability analysis can be performed:

1) For the solution ϵ_L^*:
   a) When $0 < \epsilon < \epsilon_L^*$, $\tilde{\epsilon} < 0$ and $F(\epsilon) - F(\epsilon_L^*) < 0$ since $\dot{F}(\epsilon) > 0$, and hence $\dot{V} > 0$.
   b) When $\epsilon_L^* < \epsilon < \epsilon_{MPP}$, $\tilde{\epsilon} > 0$ and $F(\epsilon) - F(\epsilon_L^*) > 0$ since $\dot{F}(\epsilon) > 0$, and hence $\dot{V} > 0$.
2) For the solution ϵ_R^*:
   a) When $\epsilon_{MPP} < \epsilon < \epsilon_H^*$, $\tilde{\epsilon} < 0$ and $F(\epsilon) - F(\epsilon_H^*) > 0$ since $\dot{F}(\epsilon) < 0$, and hence $\dot{V} < 0$.
   b) When $\epsilon_H^* < \epsilon < \epsilon_{max}$, $\tilde{\epsilon} > 0$ and $F(\epsilon) - F(\epsilon_L^*) < 0$ since $\dot{F}(\epsilon) < 0$, and hence $\dot{V} < 0$.

As a conclusion, the solution $\epsilon^* = \epsilon_L^*$ is unstable and the solution $\epsilon^* = \epsilon_R^*$ is asymptotically stable. ■

IV. Active and Reactive Power Regulation

The active and the reactive power are regulated using outer PI controllers. As Fig. 1 shows the active and the reactive power are fed back (power sensors, not depicted in the figure, are needed for that proposal) and the PI controllers generate the proper signals to compensate the required phase shifts; namely, the phase shift between the grid and the voltage at the connection point, ϕ, and the phase needed to ensure the reactive power injection, θ.

The convergence of the Lyapunov function used in the proof of the stability of the passivity-based control is ensured although the variables θ and A_I were smooth time-variants and the designer can consider that $z_2 = \xi_2$ and $z_1 = \xi_1$. Therefore, the PV inverter operates in the steady-state framework of its state variables. In order to perform a stability analysis of the power control system an equivalent model in terms of power is obtained as it is detailed in the following. Under the aforementioned assumptions, the control signals u_P and u_Q, see Fig. 1, are given by $u_P = \frac{A_{CP}A_I}{2}\cos(\varphi)$ and $u_Q = \frac{A_{CP}A_I}{2}\sin(\varphi)$ and they could be considered as some type of input power. Recalling that $\varphi = \theta + \phi$, since both the voltage at the connection point and the delivered current have a ϕ phase shift with respect to the ideal sinusoidal source, v_g, and applying some trigonometry properties, one can easily get the active and reactive powers as function of the control signals u_P and u_Q:

$$P = u_P\cos(\phi) + u_Q\sin(\phi), \tag{13a}$$

$$Q = u_Q\cos(\phi) - u_P\sin(\phi). \tag{13b}$$

Remark 2: The angle ϕ is the phase shift required to fulfil the PV inverter output network equation, which is given by

$$v_{CP} = v_{Z_g} + v_g, \tag{14}$$

where $v_{Z_g} = A_I|Z_g|\sin(\omega t - \theta + \theta_{Z_g})$ and $v_g = A\sin(\omega t + \phi)$. Therefore, ϕ depends on P, Q and Z_g.

Consequently, the overall control system can be modelled by the scheme shown in the Fig. 2.

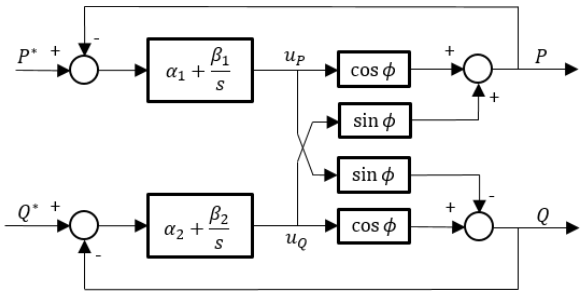

Fig. 2. Simplified scheme of the control of a PV inverter connected to a non-ideal grid.

Defining the variables: $\dot{x}_1 = P^* - P$ and $\dot{x}_2 = Q^* - Q$, it is straightforward to show that the dynamics of the system depicted in Fig. 2 are given by:

$$\mu(\phi)\dot{x}_1 = f_1(\phi) - \beta_1(\alpha_2 + \cos(\phi))x_1 - \beta_2\sin(\phi)x_2, \quad (15a)$$

$$\mu(\phi)\dot{x}_2 = f_2(\phi) - \beta_2(\alpha_1 + \cos(\phi))x_2 + \beta_1\sin(\phi)x_1, \quad (15b)$$

where $\mu(\phi) = 1 + \alpha_1\alpha_2 + (\alpha_1 + \alpha_2)\cos(\phi)$, $f_1(\phi) = (1 + \alpha_2\cos(\phi))P^* - \alpha_2\sin(\phi)Q^*$ and $f_2(\phi) = (1 + \alpha_1\cos(\phi))Q^* + \alpha_1\sin(\phi)P^*$.

At equilibrium $P = P^*$, $Q = Q^*$ and $\phi = \phi^*$, and expressions (16) are fulfilled.

$$\beta_1 x_1^* = P^*\cos(\phi^*) - Q^*\sin(\phi^*), \quad (16a)$$

$$\beta_2 x_2^* = Q^*\cos(\phi^*) + P^*\sin(\phi^*). \quad (16b)$$

Therefore, defining the variables $\tilde{x}_1 = x_1 - x_1^*$ and $\tilde{x}_2 = x_2 - x_2^*$, the dynamics characterized by (15) can be also described by:

$$\mu(\phi)\dot{\tilde{x}}_1 = F_1(\phi) - \beta_1(\alpha_2 + \cos(\phi))\tilde{x}_1 - \beta_2\sin(\phi)\tilde{x}_2, \quad (17a)$$

$$\mu(\phi)\dot{\tilde{x}}_2 = F_2(\phi) - \beta_2(\alpha_1 + \cos(\phi))\tilde{x}_2 + \beta_1\sin(\phi)\tilde{x}_1, \quad (17b)$$

where

$$F_1(\phi) = (1 - \cos(\Delta\phi) + \alpha_2\Delta\cos)P^* - (\alpha_2\Delta\sin + \sin(\Delta\phi))Q^*,$$

$$F_2(\phi) = (1 - \cos(\Delta\phi) + \alpha_1\Delta\cos)Q^* + (\sin(\Delta\phi) + \alpha_1\Delta\sin)P^*,$$

and $\Delta\cos = \cos(\phi) - \cos(\phi^*)$, $\Delta\sin = \sin(\phi) - \sin(\phi^*)$, $\Delta\phi = \phi - \phi^*$. The system described by (17) is nonlinear due to the dependence of ϕ on P and Q. Numerical analysis of (14) shows that ϕ has low variation around its equilibrium value, ϕ^*. As a consequence, in a first approach, the designer can consider that $\phi \approx \phi^*$ and, hence, $\Delta\phi = 0$, $\Delta\cos = 0$ and $\Delta\sin = 0$, and the system defined in (17) is reduced to the following linear time-invariant system:

$$\mu(\phi^*)\dot{\tilde{x}}_1 = -\beta_1(\alpha_2 + \cos(\phi^*))\tilde{x}_1 - \beta_2\sin(\phi^*)\tilde{x}_2, \quad (18a)$$

$$\mu(\phi^*)\dot{\tilde{x}}_2 = -\beta_2(\alpha_1 + \cos(\phi^*))\tilde{x}_2 + \beta_1\sin(\phi^*)\tilde{x}_1. \quad (18b)$$

Assuming $\alpha_1, \alpha_2, \beta_1, \beta_2 > 0$, the local asymptotic stability is ensured when $\beta_1(\alpha_2 + \cos(\phi^*)) + \beta_2(\alpha_1 + \cos(\phi^*)) > 0$. Notice also that the parameter ϕ^* depends on the grid impedance, Z_g, as remark 2 stated, and, therefore, the design of the PI control parameters guaranties that the closed-loop system is local asymptotically stable for the range of variation of Z_g. Furthermore, the linear system defined by (18) can be used to design the parameters of the PI controllers to provide a good behaviour for a given range of Z_g.

Remark 3: A more appropriate analysis would consider (18) as a linear time-varying system. We currently study the parameter varying analysis.

V. Simulation results

In order to validate the control, the controlled system is tested using Matlab-Simulink. For the simulation we consider the PV inverter of the Fig. 1 with $C = 2.2mF$, $L = 950\mu H$, $v_g = 312\sin(100\pi t)V$ and a PV array with a peak power of $3.3kW$, a short circuit current of $6.1A$, and an open circuit voltage of $678V$ at $1000W/m^2$ ($\Lambda = 6.1$, $\alpha = 0.026$, $\Psi = 1.35e^{-7}$. The control parameter r_a is set to 1. The transfer functions of the PI controllers are $G_{PI}(s) = 0.5 + 10/s$ for both the active and the reactive power controllers. The PV inverter is connected to a grid with an equivalent impedance of a series connection of an inductance ($L_g = 2mH$) and a resistance ($R_g = 2\Omega$). Three different tests have been developed to evaluate the control performance; namely, the first test validates the proper tracking of the power references, the second shows the robustness of the control with respect to irradiance changes and the third one confirms the control robustness with respect to the grid impedance variations.

A. Test 1: Power reference variation

Figure 3 shows the PV power, the active power and the reactive power when the system is tested when the active power and the reactive power are regulated to $P^* = 2kW$ and $Q^* = -2KVAr$, respectively. In $t = 0.6s$ the references are changed to $P^* = 3kW$ and $Q^* = -1KVAr$. The

ripple observed in the graph of the active power is because of the time interval of one grid period of the power measurement needed to synchronize the new phase shift value. As expected, the active and the reactive power are properly regulated with some dynamics close to the ones characterized by (18). This is confirmed by the Fig. 3, where the results of (18), P_{model} and Q_{model}, are added to the plot of the active and the reactive power, P and Q, of the overall controlled PV system. Notice that for $t < 0.6s$, $\phi^* = -5.6^o$, whereas for $t > 0.6s$, $\phi^* = -4.18^o$.

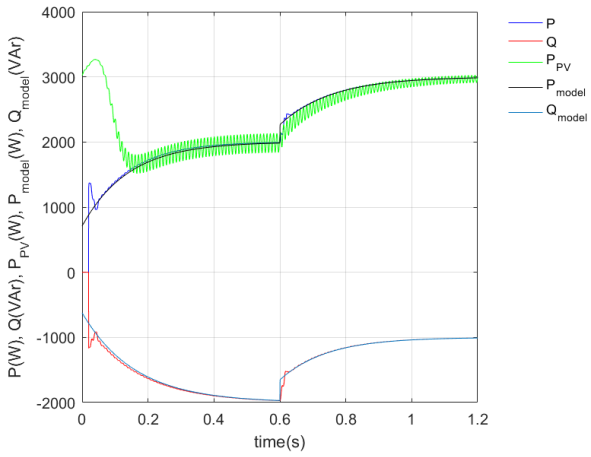

Fig. 3. Power reference variation: PV power (W), P (W) and Q (VAr).

B. Test 2: Power regulation when irradiance changes

The parameter Λ of the PV current is directly proportional to the value of the irradiance. The Fig. 4 shows the simulation results when the active power and the reactive power are regulated to $P^* = 2kW$ and $Q^* = -2KVAr$, respectively, and the irradiance varies from the initial value of $1000W/m^2$ to $750W/m^2$ in $t = 0.6s$, and reversely in $t = 1s$. Notice how the active and the reactive power are properly regulated to their reference values without any transient when the irradiance changes. The Fig. 5 depicts the power trajectories and one can realized how the PV array recovers the power point of $2kW$ after the change of irradiance.

C. Test 3: Robustness with respect to grid impedance variations

This test is devoted to show the robustness of the control when the impedance changes. Fig. 6 presents the patterns of variation of the resistive (bottom view) and the inductive (top view) components of the grid impedance. Fig. 7 shows the PV power, the active power and the reactive

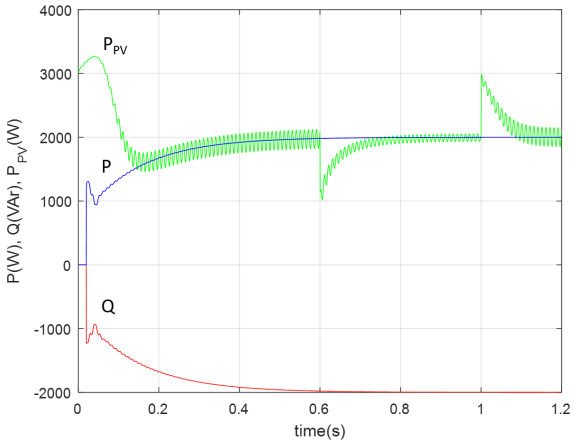

Fig. 4. Irradiance changes: PV power (W), P (W) and Q (VAr).

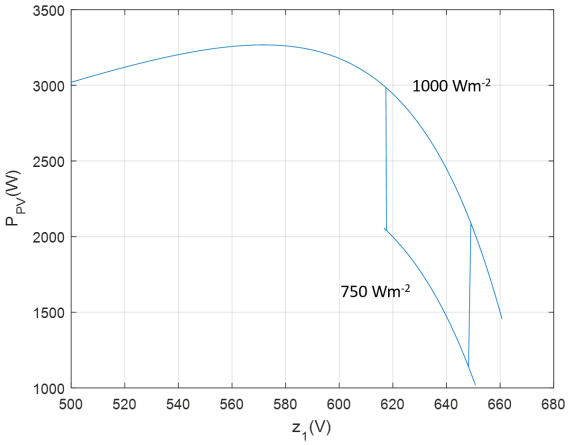

Fig. 5. Irradiance changes: PV power (W) versus z_1 (V) curves.

power behaviours in the test. The active and reactive power references are of $P^* = 2kW$ and $Q^* = -2kVA$. Notice how, as expected from the previous analysis, the active and reactive powers always reach their references values and suffers smooth and brief transients when the resistive or the reactive components of the grid impedance varies.

VI. Conclusions

The design of a control to regulate the active and the reactive power in single-phase PV inverters is presented in this work. The control is composed by two different loops. The inner loop is a passivity-based control for tracking the reference current. The proof of the global asymptotic convergence of the tracking error to zero is provided. The outer loop uses PI controllers in charge to regulate the active

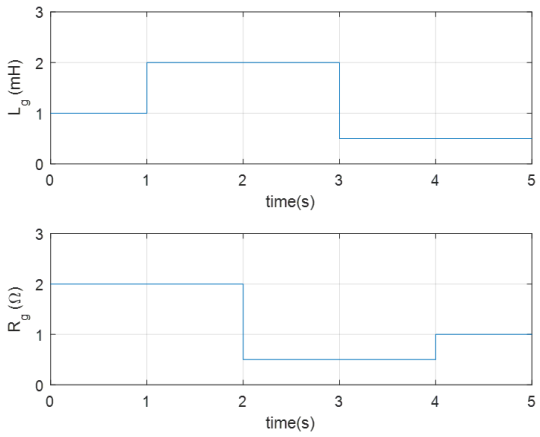

Fig. 6. Impedance variations: top plot, L_g (mH), bottom plot, R_g (Ω).

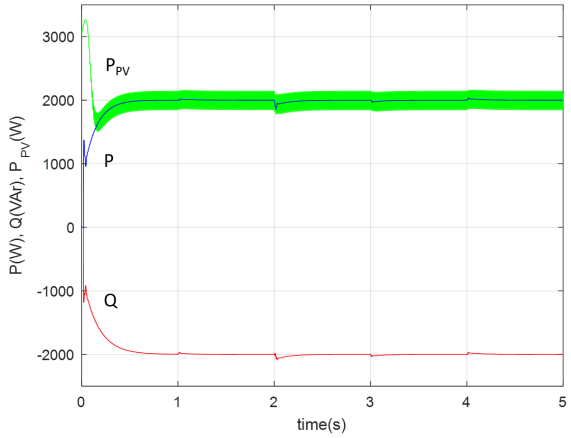

Fig. 7. Impedance variations: PV power (W), P (W) and Q (VAr).

and the reactive power and provides robustness with respect to the unknown grid impedance. A model of the overall controlled system is obtained and the PI parameters design guidelines that ensure local asymptotic stability are also given. Numerical simulations confirm the expected stability and show a good current tracking with fast dynamics and robustness with respect to the PV irradiance changes and grid impedance variations.

VII. Acknowledgments

This work is partially supported by the Project DPI2017-85404-P.

References

[1] A. Bonfiglio, M. Brignone, F. Delfino, R. Procopio, "Optimal Control and Operation of Grid-Connected Photovoltaic Production Units for Voltage Support in Medium-Voltage Networks," *in IEEE Transactions on Sustainable Energy*, January 2014.

[2] A. Cagnano, E. De Tuglie, M. Liserre, R.A. Mastromauro, "Online Optimal Reactive Power Control Strategy of PV Inverters," *in IEEE Transactions on Industrial Electronics*, October 2011.

[3] V.N. Lal, S.N. Singh, "Control and Performance Analysis of a Single-Stage Utility-Scale Grid-Connected PV System," *in IEEE Systems Journal*, in press.

[4] A. Anurag, Y. Yang, F. Blaabjerg, "Thermal Performance and Reliability Analysis of Single-Phase PV Inverters With Reactive Power Injection Outside Feed-In Operating Hours," *in IEEE Journal of Emerging and Selected Topics in Power Electronics*, December 2015.

[5] Y. Yang, H. Wang, F. Blaabjerg, "Reactive Power Injection Strategies for Single-Phase Photovoltaic Systems Considering Grid Requirements," *in IEEE Transactions on Industry Applications*, November-December 2014.

[6] Y. Yang, F. Blaabjerg, H. Wang, M.G. Simoes, "Power control flexibilities for grid-connected multi-functional photovoltaic inverters," *in IET Renewable Power Generation*, October 2016.

[7] R.I. Bojoi, L.R. Limongi, D. Roiu, A. Tenconi, "Enhanced Power Quality Control Strategy for Single-Phase Inverters in Distributed Generation Systems," *in IEEE Transactions on Power Electronics*, March 2011.

[8] W. Sripipat, S. Po-Ngam, "Simplified active power and reactive power control with MPPT for single-phase grid-connected photovoltaic inverters," *in Proc. Electrical Engineering/Electronics, Computer, Telecommunications and Information Technology*, 2014.

[9] Y. Yang, F. Blaabjerg, H. Wang, "Low-Voltage Ride-Through of Single-Phase Transformerless Photovoltaic Inverters," *in IEEE Transactions on Industry Applications*, May-June 2014.

[10] S. Dasgupta, S.K. Sahoo, S.K. Panda, "Single-Phase Inverter Control Techniques for Interfacing Renewable Energy Sources With MicrogridPart I: Parallel-Connected Inverter Topology With Active and Reactive Power Flow Control Along With Grid Current Shaping," *in IEEE Transactions on Power Electronics*, March 2011.

[11] D. Biel, J.M.A. Scherpen, "Passivity-based control of active and reactive power in single-phase PV inverters," *in Proc. 26th IEEE International Symposium on Industrial Electronics*, June 2017.

[12] R. Ortega, J.A. Loira Perez, P.J. Nicklasson, H. Sira-Ramirez, *Passivity-based Control of Euler-Lagrange Systems*, Springer; 1998.

[13] D. Jeltsema, J.M.A. Scherpen. "Tuning of Passivity-Preserving Controllers for Switched-Mode Power Converters," *in IEEE Transactions on Automatic Control*, August 2004.

[14] C. Meza, D. Biel, D. Jeltsema, J.M.A. Scherpen. "Lyapunov-Based Control Scheme for Single-Phase Grid-Connected PV Central Inverters," *in IEEE Transactions on Control Systems Technology*, March 2012.

[15] D. del Puerto-Flores, J.M.A. Scherpen, M. Liserre, M.M.J. de Vries, M.J. Kransse, V.G. Monopoli, "Passivity-Based Control by Series/Parallel Damping of Single-Phase PWM Voltage Source Converter," *in IEEE Transactions on Control Systems Technology*, 2014.

[16] H. Komurcugil, "Steady-State Analysis and Passivity-Based Control of Single-Phase PWM Current-Source Inverters," *in IEEE Transactions on Industrial Electronics*, March 2010.

[17] A. Dell'Aquila, M. Liserre, V.G. Monopoli, C. Cecati, "Passivity-based control of a single-phase H-bridge multilevel active rectifier," *in Proc. IEEE Annual Conference of the Industrial Electronics Society*, 2002.

[18] A.F. Cupertino, J.T. de Resende, H.A. Pereira, S.I. Seleme Jnior, "A grid-connected photovoltaic system with a maximum power point tracker using passivity-based control applied in a boost converter," *in Proc. IEEE/IAS International Conference on Industry Applications*, 2012.